Attachment of bacteriophages MS2 and ΦX174 onto kaolinite and montmorillonite: Extended-DLVO interactions

ARTICLE *in* COLLOIDS AND SURFACES B: BIOINTERFACES · NOVEMBER 2011

Impact Factor: 4.15 · DOI: 10.1016/j.colsurfb.2011.11.028 · Source: PubMed

2 AUTHORS:

Constantinos V. Chrysikopoulos
Technical University of Crete
143 PUBLICATIONS **2,004** CITATIONS
SEE PROFILE

Vasiliki Syngouna
University of Patras
22 PUBLICATIONS **147** CITATIONS
SEE PROFILE

Colloids and Surfaces B: Biointerfaces 92 (2012) 74–83

Contents lists available at SciVerse ScienceDirect

Colloids and Surfaces B: Biointerfaces

journal homepage: www.elsevier.com/locate/colsurfb

Attachment of bacteriophages MS2 and ΦX174 onto kaolinite and montmorillonite: Extended-DLVO interactions

Constantinos V. Chrysikopoulos*, Vasiliki I. Syngouna

Environmental Engineering Laboratory, Department of Civil Engineering, University of Patras, Patras 26500, Greece

ARTICLE INFO

Article history:
Received 27 July 2011
Received in revised form 18 October 2011
Accepted 11 November 2011
Available online 22 November 2011

Keywords:
ΦX174
MS2
Clay minerals
KGa-1b
STx-1b
Virus attachment
Colloid stability
Extended DLVO
Hydrophobic force

ABSTRACT

This study aims to gain insights into the interaction of virus particles with clay colloids. Bacteriophages MS2 and ΦX174 were used as model viruses and kaolinite (KGa-1b) and montmorillonite (STx-1b) as model colloids. The experimental data obtained from batch experiments of MS2 and ΦX174 attachment onto KGa-1b and STx-1b suggested that virus attachment is adequately described by the Freundlich isotherm equation. Both MS2 and ΦX174 were attached in greater amounts onto KGa-1b than STx-1b with MS2 having greater affinity than ΦX174 for both clays. Furthermore, extended-DLVO interaction energy calculations explained that the attachment of viruses onto model clay colloids was primarily caused by hydrophobic interaction. The theoretical and experimental results of this study were found to be in good agreement with previous findings.

1. Introduction

Pathogenic viruses present in groundwater are likely to originate from accidental (landfills, broken sewer pipelines, leaking septic tanks, graveyards, urban runoff, irrigation) and intentional (direct injection wells, recharge basins) pollution sources [1–3]. Clay minerals are the finest inorganic components in soils and sediments and occur naturally in groundwater. Clay minerals have a very high surface area to volume ratio and great affinity for contaminants and biocolloids (viruses and bacteria) [4–8]. Therefore, suspended clay minerals are instrumental in providing contaminants and biocolloids with the opportunity to migrate while sorbed or attached onto their surfaces [9,10]. Numerous studies have provided evidence that contaminants as well as biocoloids sorb or attach onto suspended colloids and can migrate substantially farther than in the absence of mobile colloids [11–24].

The transport of viruses in porous and fractured subsurface environments is governed by numerous factors including virus inactivation, temperature, and water chemistry [25–29], and has been investigated extensively theoretically [30–35] as well as experimentally at the laboratory [36–43] and at the field scale [2,44–48]. Although the attachment of viruses onto clay minerals has been examined by a number of investigators [7,49–51], more work is needed in order to fully understand and precisely define the fundamental mechanisms governing virus attachment onto the various clay minerals commonly found in groundwater.

Colloid stability is often predicted by the Derjaguin–Landau–Verwey–Overbeek (DLVO) theory [52,53], which was developed for smooth, homogeneous particles with ideal geometries. However, the majority of the colloids found in the subsurface are of irregular geometries with rough surfaces and heterogeneous composition. Despite the success of DLVO theory, numerous investigators have modified the DLVO theory to include factors not accounted for in the DLVO model. The extended-DLVO (XDLVO) theory includes the magnitude of the Lewis acid–base interaction [54,55]. The XDLVO theory is currently the subject of much research and discussion [40,56].

In the present study, batch experiments were conducted to characterize the attachment of viruses onto clay colloids by extending the research efforts by Syngouna and Chrysikopoulos [7], who studied the effect of temperature and agitation on the interactions of MS2 and ΦX174 with untreated, "readily available" kaolinite and bentonite (90% montmorillonite) under quite different experimental and analytical procedures than those employed here. The extended-DLVO approach was used to evaluate the attachment of bacteriophages MS2 and ΦX174 onto well-crystallized kaolinite (KGa-1b) and montmorillonite (STx-1b) (colloidal fraction <2 μm). Furthermore, the surface properties of viruses and clays were

* Corresponding author. Tel.: +30 6945373208; fax: +30 2610996573.
E-mail address: gios@upatras.gr (C.V. Chrysikopoulos).

0927-7765/$ – see front matter © 2011 Elsevier B.V. All rights reserved.
doi:10.1016/j.colsurfb.2011.11.028

Nomenclature

A	absorbance (–)
A_{ii}	Hamaker constant of individual component, $M{\cdot}L^2/t^2$
A_{ijk}	combined Hamaker constant, $M{\cdot}L^2/t^2$
C_i	aqueous phase concentration of species i, M/L
C_{i_o}	initial aqueous phase concentration of species i, M/L
C^*	concentration of viruses attached onto clay colloids, (M viruses)/(M clay)
e	elementary charge (C)
h	separation distance between two approaching surfaces, L
h_o	minimum separation distance between two approaching surfaces, L
i	subscript indicating the various materials used in this study
I_s	ionic strength (mol/L)
k_B	Boltzman's constant, $M{\cdot}L^2/(t^2{\cdot}K)$
K_f	Freundlich constant, $(L^3/M)^m$
K_{123}	hydrophobic force constant (J), $M{\cdot}L^2/t^2$
m	Freundlich exponent (–)
N_A	Avogadro's number (1/mol)
r_p	average colloidal particle radius, L
T	Temperature (K), T
β_i	contact angle of material i (°)
ε	dielectric constant of the suspending liquid ($C^2/(J\,m)$)
ε_0	permittivity of free space ($C^2/(J\,m)$)
ε_r	relative dielectric constant of the suspending liquid (–)
θ	XRD scanning angle increment (°)
κ	Debye–Huckel parameter, 1/L
λ	characteristic wavelength of interaction between two approaching surfaces, L
λ_{AB}	decay (Debye) length of water, L
σ_{Born}	Born collision parameter, L
Φ_{AB}	Lewis acid-base potential energy (J), $M{\cdot}L^2/t^2$
$\Phi_{AB(h_o)}$	Lewis acid–base free energy of interaction at $h = h_o$ (J/m^2), M/t^2
Φ_{Born}	Born potential energy (J), $M{\cdot}L^2/t^2$
Φ_{dl}	double layer potential energy (J), $M{\cdot}L^2/t^2$
Φ_{max1}	primary maximum of Φ_{tot} (J), $M{\cdot}L^2/t^2$
Φ_{min1}	primary minimum of Φ_{tot} (J), $M{\cdot}L^2/t^2$
Φ_{min2}	secondary minimum of Φ_{tot} (J), $M{\cdot}L^2/t^2$
Φ_{vdW}	van der Waals potential energy (J), $M{\cdot}L^2/t^2$
Ψ_p	surface potential of the colloid particle (V)
Ψ_s	surface potential of the collector surface (V)

evaluated by electrophoretic mobility measurements and were used for the construction of DLVO and XDLVO potential energy profiles.

2. Materials and methods

2.1. Bacteriophages and assay

The bacteriophages MS2 (an F-specific single-stranded RNA phage with effective particle diameter ranging from 24 to 26 nm) and ΦX174 (a somatic single-stranded DNA phage with effective particle diameter ranging from 25 to 27 nm), were used in this study as surrogates for human viruses. MS2 has a hydrophobic protein coat, and ΦX174 has a hydrophilic protein coat [57]. Both bacteriophages infect *E coli*, and were assayed by the double-layer overlay method [58], as outlined by Syngouna and Chrysikopoulos [43].

For the separation of viruses adsorbed onto clay colloids from suspended viruses in the liquid phase, in 2 mL of the liquid sample was added 0.3 mL of the density gradient separation reagent Histodenz (60% by weight, AXIS-SHIELD PoC AS Company, Norway) [5,6,10]. The mixture was centrifuged at 2000 × *g* for 30 min so that the supernatant was free of clay colloids. The optimum separation conditions were determined experimentally. The suspension of unattached viruses in the supernatant was pipetted out and the suspended viruses were determined by the double-layer overlay method [58]. The absence of clay colloids in the supernatant was verified by a UV–vis spectrophotometer (UV-1100, Hitachi) at a wavelength of 280 nm. The concentration of attached viruses was determined by subtracting the mass of viruses that remained in suspension from the initial virus concentration in each sample. In addition, preliminary control experiments were conducted, as outlined by Vasiliadou and Chrysikopoulos [10], to verify that Histodenz did not interfere with the virus concentration measurements.

2.2. Clays

The clays used in this study were kaolinite (KGa-1b, is a well-crystallized kaolin from Washington County, Georgia [59]) and montmorillonite (STx-1b, a Ca-rich montmorillonite, white, from Gonzales County, Texas), purchased from the Clay Minerals Society, Columbia, USA. KGa-1b has a specific surface area of 10.1 m^2/g, as evaluated by the Brunauer–Emmet–Teller (BET) method, and a cation exchange capacity of 2.0 meq/100 g [60]. STx-1b has a specific surface area of 82.9 m^2/g [61], and assuming that the characteristics of STx-1b are comparable to those of STx-1, which is the previous batch of montmorillonite from the same area, its cation exchange capacity is 84.4 meq/100 g [60].

Fifty grams of each clay mineral were mixed with 100 mL distilled deionized water (ddH_2O) in a 2 L beaker. Sufficient hydrogen peroxide (30%, solution) was added to oxidize all organic matter. The mineral suspension was adjusted to pH 10 with 0.1 M NaOH solutions and dispersed by ultrasonication for 20 min. The suspension was diluted to 2 L and the <2 μm colloidal fraction was separated by sedimentation. The separated colloid suspension was flocculated by adding 0.5 M $CaCl_2$ solution. The colloidal particles were washed with ddH_2O and ethanol to remove the Cl^- ions and subsequently dried at 60 °C [6]. The optical density of the clay colloids was analyzed at a wavelength of 280 nm by a UV–vis spectrophotometer, and the corresponding clay concentrations were calibrated with the standard curves of clay optical densities presented in Fig. 1, which are based on dry weights. Using the calibration curves (Fig. 1), each measured KGa-1b absorbance, $A_{(KGa\text{-}1b)}$ [–], was converted to KGa-1b concentration, $C_{(KGa\text{-}1b)}$ [g/L], using the relationship:

$$C_{(KGa-1b)} = 0.314\,A_{(KGa-1b)} + 0.026 \quad (1)$$

Similarly, each measured STx-1b absorbance, $A_{(STx\text{-}1b)}$ [–], was converted to STx-1b concentration, $C_{(STx\text{-}1b)}$ [g/L], using the relationship:

$$C_{(STx-1b)} = 0.326A_{(STx-1b)} - 0.007 \quad (2)$$

Note that the absorbance was assumed to be a non-dimensional number as recorded by the spectrophotometer.

Transmission electron microscopy (TEM) by a JEOL (JEM-2100 system, operated at 200 kV) was performed by diluting each clay colloid fraction <2 μm in ddH_2O, placed in an ultrasonic bath for 10 min, and air-dried onto a carbon-coated copper grid (200 mesh). Micrograph images were recorded by a Erlangshen CCD Camera (Model 782 ES500W). Two representative images are shown in Fig. 2. The TEM analyses suggested that KGa-1b was dominated by kaolinite hexagonal platy particles with size in the range of

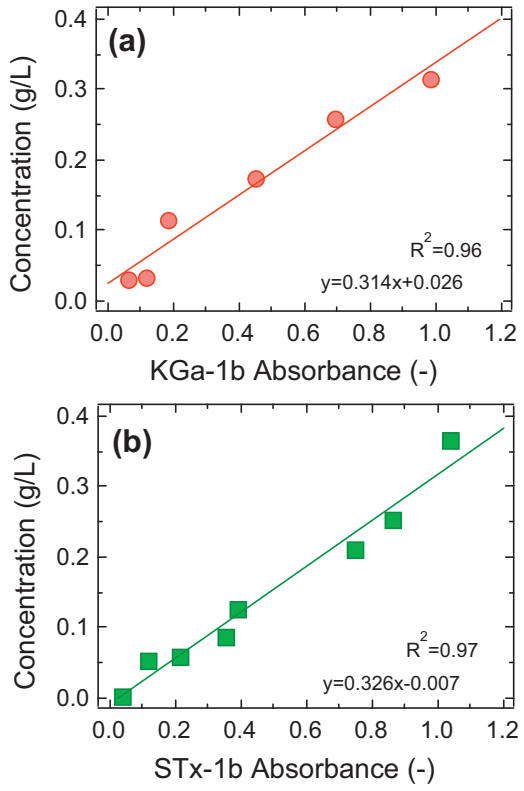

Fig. 1. Concentration calibration curves for (a) KGa-1b, and (b) STx-1b.

0.2–1 μm and traces of anatase (see Fig. 2a), and that STx-1b was dominated by montmorillonite irregular thin flaky particles with average size 0.5 μm (see Fig. 2b).

The mineralogical composition of KGa-1b and STx-1b, "as shipped" (or untreated), were determined by X-ray diffraction (XRD) using a Bruker D8 advance diffractometer, with Ni-filtered CuKα radiation and a LynxEye detector. XRD patterns were obtained at a 2θ range from 2° to 70°, scanned at a scanning angle increment of 0.015° with a time step of 0.3 s. The XRD patterns shown in Fig. 3 indicated that KGa-1b is very pure kaolinite with some traces of anatase and illite (mica) (see Fig. 3a), and STx-1b contains mostly montmorillonite (smectite) with some traces of quartz and illite (mica) (see Fig. 3b).

Scanning electron microscopy (SEM) coupled with energy dispersive spectrometer (EDS) also carried out for morphology and chemical composition of the clays. Dried clay samples (<2 μm colloidal fraction) were gold coated for morphological observation and carbon coated for chemical analysis SEM (JEOL-6300 microscope) with EDS (OXFORD, Link PentaFet) analysis was performed at 20 kV. EDS is an analytical technique, which utilizes X-rays that are emitted from the specimen when bombarded by the electron beam to identify the elemental composition of the specimen. The scanning electron micrograms are shown in Fig. 4 and the chemical composition of the clays are listed in Table 1 together with the chemical composition for KGa-1 and STx-1 reported by van Olphen and Fripiat [60]. Clearly, the chemical composition for KGa-1b and STx-1b obtained in this study are similar to those reported by van Olphen and Fripiat [60] for KGa-1 and STx-1, respectively.

2.3. Electrokinetic measurements

The Zeta potentials of the bacteriophages and clays used in this study were measured at pH 7 in ddH_2O by a zetasizer (Nano ZS90, Malvern Instruments, Southborough, MA). The zeta potentials were determined to be -40.4 ± 3.7 mV for MS2, -31.78 ± 1.25 mV for ΦX174, -26.03 ± 2.77 mV for KGa-1b, and -20.5 ± 0.8 mV for STx-1b. The isoelectric point (IEP), which represents the pH where the electrophoretic mobility changes from positive to negative, for the bacteriophages and clays used in this study were determined by diluting bacteriophage stocks and clay colloids in ddH_2O water and varying the pH from 2.5 to 11 with 0.1 M HNO_3 and 0.1 M NaOH. The measured Zeta potentials are shown in Fig. 5. The IEP of MS2, ΦX174, and KGa-1b in ddH_2O were found to be equal to $pH_{IEP} = 4.1$, 4.4, and 2.1, respectively. Please note that zeta potential of STx-1b is negative in the pH range examined. Furthermore, the zetasizer was used to measure the hydrodynamic diameter of the clay particles, which were found to be equal to 842.85 ± 125.85 nm for KGa-1b, and 1187 ± 380.81 nm for STx-1b. All zeta potential and hydrodynamic diameter measurements were obtained in triplicates.

2.4. Batch experiments

The attachment of MS2 and ΦX174 onto both KGa-1b and STx-1b clay particles was investigated with batch equilibration experiments conducted over a 7 h time period. The equilibration time was selected to be short enough so that minimum or no virus inactivation occurred. Furthermore, preliminary experiments

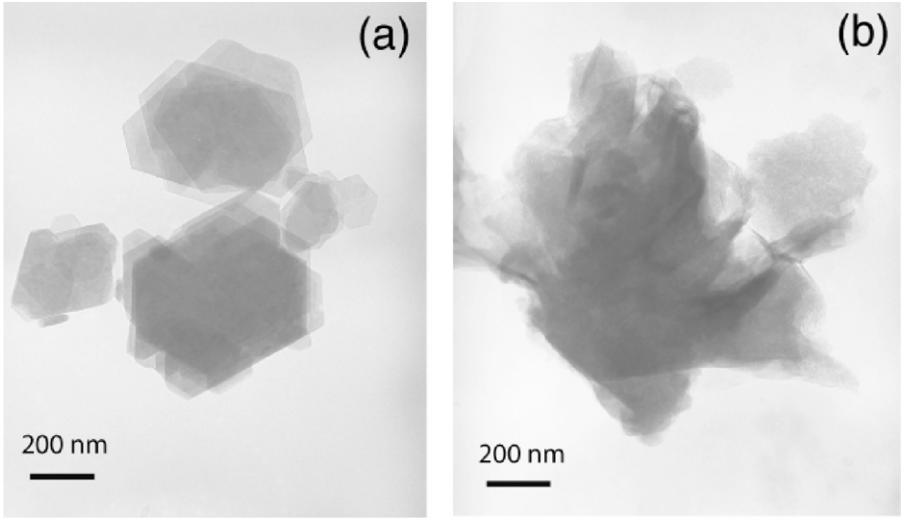

Fig. 2. Transmission electron micrographs of (a) KGa-1b, and (b) STx-1b.

Table 1
Chemical composition of clay samples (wt.%, not including H_2O).

	KGa-1b (wt.%)[a]	KGa-1 (wt.%)[b]	STx-1b (wt.%)[a]	STx-1 (wt .%)[b]
SiO_2	45.41	44.2	72.92	70.1
Al_2O_3	38.79	39.7	15.34	16.0
TiO_2	0.28	1.39	0.13	0.22
Fe_2O_3	0.21	0.13	0.75	0.65
FeO	–	0.08	–	0.15
MnO	–	0.002	0.17	0.009
MgO	0.01	0.03	3.69	3.69
CaO	–	n.d.	1.61	1.59
Na_2O	0.21	0.013	0.29	0.27
K_2O	0.2	0.05	0.10	0.078
P_2O_5	–	0.034	0.05	0.026
F			–	0.084
S			0.05	0.04

[a] EDS analysis (this study).
[b] van Olphen and Fripiat [60].

showed that equilibrium was reached within just a 3 h time period. The method consisted of adding virus stock solution to a 50 mL centrifuge tube containing a selected clay colloid concentration (113.579 ± 25 mg/L of KGa-1b or 160 ± 6.5 mg/L of STx-1b), after sealing, the centrifuge tubes were gently shaked for 7 h at 25 °C. Different virus concentrations, ranging from 10^3 to 10^9 PFU/mL were used. Each concentration collected from the same virus stock solution, was diluted with ddH_2O. Sub-samples of 2 mL were withdrawn from each centrifuge tube at regular intervals to determine the concentration of viruses attached onto clay colloids. Furthermore, control tubes, in the absence of clays, were used to monitor the inactivation of the two viruses. The experimental data are shown in Fig. 6 and suggest that no significant virus inactivation occurred during the experimental time period. The control tubes received only virus solution in ddH_2O and were treated in the same manner as the reactor tubes for the virus attachment experiments.

3. Theoretical considerations

3.1. Virus–clay colloid interactions

The classical DLVO theory treats the total interaction energy between two smooth, homogeneous surfaces with ideal geometries as the sum of an attractive energy due to van der Waals forces, an electrostatic repulsion energy arising from the overlap of electrical double layers, and at very close separation distances the Born repulsion energy due to overlapping electron orbitals of the molecules comprising the different surfaces. Consequently, based on the classical DLVO theory, the total interaction energy between two surfaces equals the arithmetic sum of the van der Waals, Φ_{vdW}, double layer, Φ_{dl}, and Born, Φ_{Born}, potential energies [62]:

$$\Phi_{DLVO}(h) = \Phi_{vdW}(h) + \Phi_{dl}(h) + \Phi_{Born}(h) \quad (3)$$

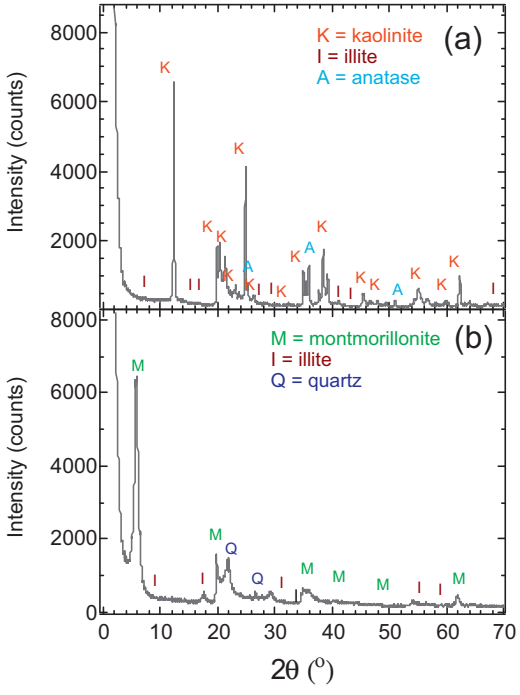

Fig. 3. X-ray diffraction patterns of (a) KGa-1b, and (b) STx-1b.

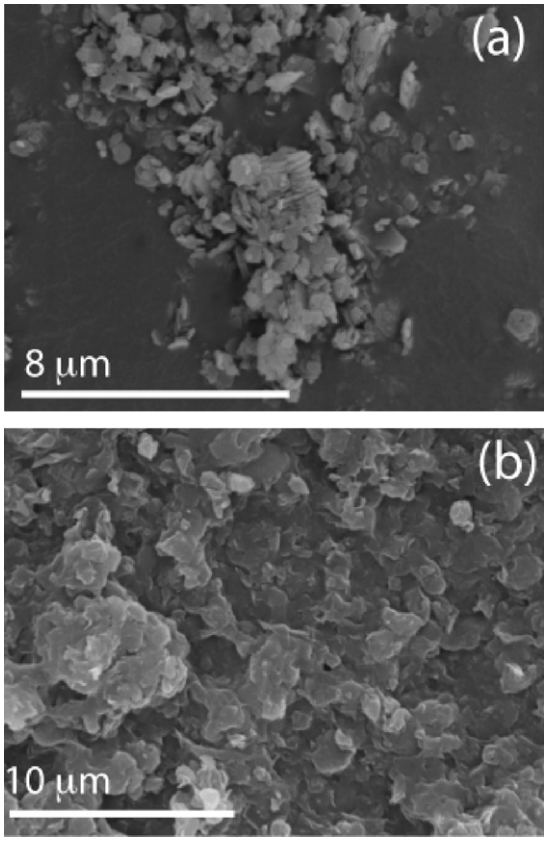

Fig. 4. Scanning electron micrographs of (a) KGa-1b, and (b) STx-1b.

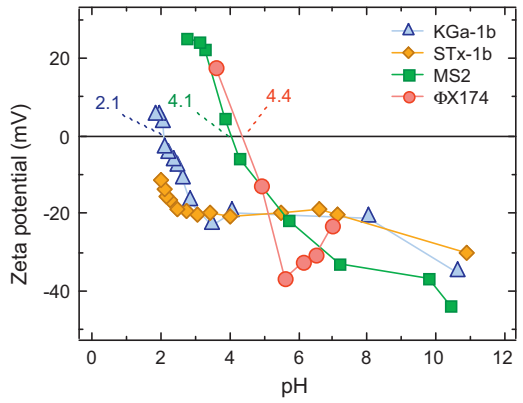

Fig. 5. Zeta potential as a function of solution pH for KGa-1b (triangles), STx-1b (diamonds), MS2 (squares), and ΦX174 (circles) in ddH_2O at 25 °C.

where h [m] is the separation distance between the approaching surfaces.

3.1.1. Sphere–plate particle geometries

For the case of two approaching surfaces, one with spherical and the other with planar geometries (sphere–plate), the Φ_{vdW} [J] interactions were calculated with the following expression [63]:

$$\Phi_{vdW}(h) = -\frac{A_{123} r_p}{6h}\left[1 + \left(\frac{14h}{\lambda}\right)\right]^{-1} \quad (4)$$

where A_{123} [J] is the combined Hamaker constant for microscopic bodies of composition "1" and "3" in medium "2" [(1-colloid)-(2-water)-(3-collector)] (note that A_{121} is the combined Hamaker constant for the aggregation of two colloid particles of composition "1" suspended in a medium "2". If the medium "2" is water then the combined Hamaker constant can be written as A_{1w1}), $\lambda \approx 10^{-7}$ m is the characteristic wavelength of the sphere-plate or sphere-sphere interactions, and r_p [m] is the colloid particle radius. The combined Hamaker constant can be estimated by the following combining rule using Hamaker constants of the individual components of the system as follows [64]:

$$A_{123} = (\sqrt{A_{11}} - \sqrt{A_{22}})(\sqrt{A_{33}} - \sqrt{A_{22}}) \quad (5)$$

where A_{11}, A_{22}, and A_{33} [J] are the Hamaker constants of the three individual components. Also, the combined Hamaker constant for asymmetric dispersion interactions, A_{123}, can be estimated by the geometric mean combining rule [55],

$$A_{123} = \sqrt{A_{121} - A_{323}} \quad (6)$$

Note that the Hamaker constant is a material property and in most cases its value is quite uncertain [65]. The Φ_{dl} for sphere-late interactions were calculated with the expression [66]:

$$\Phi_{dl}(h) = \pi\varepsilon_r\varepsilon_0 r_p \left[2\Psi_p\Psi_s \ln\left(\frac{1+e^{-\kappa h}}{1-e^{-\kappa h}}\right) + (\Psi_p^2 + \Psi_s^2)\ln(1-e^{-2\kappa h})\right] \quad (7)$$

where $\varepsilon_r = \varepsilon/\varepsilon_0$ is the dimensionless relative dielectric constant of the suspending liquid, ε [$C^2/(J\,m)$] is the dielectric constant of the suspending liquid, ε_0 [$C^2/(J\,m)$] is the permittivity of free space, Ψ_p [V] is the surface potential of the colloid particle, Ψ_s [V] is the surface potential of the collector surface (plate), and κ [1/m] is the inverse of the diffuse layer thickness, known as the Debye-Huckel parameter:

$$\kappa = \left[\frac{2\,I_s\,N_A 1000 e^2}{\varepsilon_r\varepsilon_0 k_B T}\right]^{1/2} \quad (8)$$

where I_s [mol/L] is the ionic strength, $N_A = 6.02 \times 10^{23}$ [1/mol] is Avogadro's number, $e = 1.602 \times 10^{-19}$ [C] is the elementary charge, $k_B = 1.38 \times 10^{-23}$ [J/K] is the Boltzmann constant, and $T = 298$ [K] is the fluid absolute temperature. The Φ_{Born} [J] for sphere-plate was estimated by the relationship [67]:

$$\Phi_{Born}(h) = \frac{A_{123}\,\sigma_{Born}^6}{7560}\left[\frac{8r_p + h}{(2r_p + h)^7} + \frac{6r_p - h}{h^7}\right] \quad (9)$$

where σ_{Born} [m] is the Born collision parameter. For the commonly used value of $\sigma_{Born} = 5$ Å [67], the resulting acceptable minimum separation distance, at $h = h_o$, i.e. at "contact", is estimated to be $h_o \approx 2.5$ Å = 0.25 nm, which compares well to $h_o = 4$–10 Å estimated by other investigators [68,69]. Note that Φ_{Born} can easily be neglected if $h > 1$ nm. The effect of Born interaction may not be of great significance in aqueous systems since the presence of any hydrated ions, which are likely to be present, will prevent surface-surface separation distances to approach $h = 0.3$ nm.

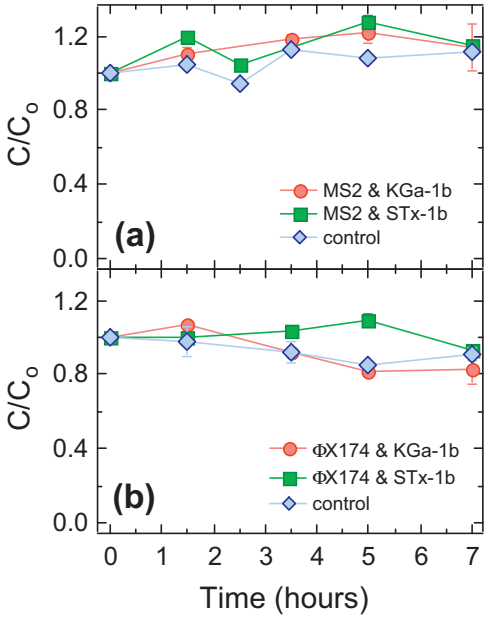

Fig. 6. Inactivation of (a) MS2, and (b) ΦX174 in the presence of KGa-1b (circles), STx-1b (squares), and control data in the absence of clays (diamonds).

3.1.2. Sphere–sphere particle geometries

For the case of sphere–sphere particle geometries, the Φ_{vdW} [J] interactions were calculated with the following expression [70,71]:

$$\Phi_{vdW}(h) = -\frac{A_{123}}{12}\left\{\frac{R_p}{\xi^2 + \xi R_p + \xi} + \frac{R_p}{\xi^2 + \xi R_p + \xi + R_p} + 2\ln\left[\frac{\xi^2 + \xi R_p + \xi}{\xi^2 + \xi R_p + \xi + R_p}\right]\right\} \quad (10)$$

where

$$R_p = \frac{r_{p2}}{r_{p1}} \quad (11)$$

$$\xi = \frac{h}{r_{p1}} \quad (12)$$

r_{p1} [m] is the radius of the spherical colloid particle 1, and r_{p2} [m] is the radius of the spherical colloid particle 2 (usually $r_{p1} \le r_{p2}$).

The Φ_{dl} [J] for sphere-sphere interactions were calculated with the expression [66]:

$$\Phi_{dl}(h) = \pi\varepsilon_r\varepsilon_0\frac{r_{p1}r_{p2}}{(r_{p1}+r_{p2})}\left[2\Psi_{p1}\Psi_{p2}\ln\left(\frac{1+e^{-\kappa h}}{1-e^{-\kappa h}}\right) + (\Psi_{p1}^2+\Psi_{p2}^2)\ln(1-e^{-2\kappa h})\right] \quad (13)$$

where Ψ_{p1} [V] is the surface potential of the colloid (virus or clay), and Ψ_{p2} [V] is the surface potential of the second sphere. The Φ_{Born} [J] for sphere–sphere interactions were estimated with the relationship [70,71]:

$$\Phi_{Born}(h) = \frac{A_{123}}{7560\xi}\left(\frac{\sigma_{Born}}{r_{p1}}\right)^2 \left[\frac{-4\xi^2-14(R_p-1)\xi-6(R_p^2-7R_p+1)}{(2\xi-1+R_p)^7} + \frac{-4\xi^2+14(R_p-1)\xi-6(R_p^2-7R_p+1)}{(2\xi+1-R_p)^7} + \frac{4\xi^2+14(R_p-1)\xi+6(R_p^2+7R_p+1)}{(2\xi+1+R_p)^7} + \frac{4\xi^2-14(R_p-1)\xi+6(R_p^2+7R_p+1)}{(2\xi-1-R_p)^7}\right] \quad (14)$$

In this study, the combined Hamaker constants for the system virus–water–virus was set to $A_{1w1} = 7.5\times10^{-21}$ J [72], for the system KGa-1b–water–KGa-1b to $A_{1w1} = 3.1\times10^{-20}$ J, and for the system STx-1b–water–STx-1b to $A_{1w1} = 2.2\times10^{-20}$ J [73].

3.2. Extended DLVO theory of colloid stability

The interaction potential energies considered in the classical DLVO theory cannot always explain successfully colloid particle interactions [54]. The discrepancy between experimental data and theory is attributed to additional energies, namely hydration pressure, hydrogen bonding forces, hydrophobic effects, disjoining pressure, structural forces, and Lewis acid–base forces [64,74–76]. These forces are attractive or repulsive and they are known to be sensitive to adsorption of ions or molecules at the interface. The non-DLVO short-range repulsive forces have been termed hydration forces, while longer-range attractive forces between hydrophobic bodies have been considered hydrophobic interactions. van Oss [54] calculated the non-DLVO forces that arise from Lewis acid–base electron donor–electron acceptor interactions between surfaces, adsorbed species, and the solvent. The incorporation of additional energies of interaction into the simple DLVO model is currently known as the extended-DLVO or XDLVO theory.

The hydrophobicity of a surface is characterized by the water contact angle, β [°]. Traditionally, materials are divided into two categories: wetting ($\beta<90°$) and non-wetting ($\beta>90°$). Worthy to note is that hydrophobic interactions between surfaces become effective at $\beta>65°$ and hydrophilic interactions at $\beta<65°$. Hydrophobic interactions are of substantial importance to virus stability behavior. The hydrophobic behavior of viruses depends on the composition of their protein coat (capsid). The capsids contain various hydrophobic amino acids, which may be either on the outside or the inside of the virus coat. Kaolinites (e.g., KGa-1b) and montmorillonites (e.g., STx-1b) are moderately hydrophilic [77,78] and have large negative zeta potentials at pH > 2 (see Fig. 5).

In this study, according to the XDLVO theory, the total interaction energy between surfaces is considered as the sum of the classical DLVO, Φ_{DLVO}, and Lewis acid–base, Φ_{AB}, interaction energies over a separation distance, h [m], between two approaching surfaces [76]:

$$\Phi_{XDLVO}(h) = \Phi_{DLVO}(h) + \Phi_{AB}(h) \quad (15)$$

The Lewis acid–base interaction energy, Φ_{AB}, decays exponentially with distance [74]. For the case of sphere–plate Φ_{AB} [J] interactions were calculated with the following relation [74,77]:

$$\Phi_{AB}(h) = 2\pi r_p\lambda_{AB}\Phi_{AB(h=h_o)}\exp\left[\frac{h_0-h}{\lambda_{AB}}\right] \quad (16)$$

and for the case of sphere-sphere with

$$\Phi_{AB}(h) = 2\pi\frac{r_{p1}r_{p2}}{r_{p1}+r_{p2}}\lambda_{AB}\Phi_{AB(h=h_0)}\exp\left[\frac{h_0-h}{\lambda_{AB}}\right] \quad (17)$$

where $\Phi_{AB(h=h_0)}$ [J/m^2] is the Lewis acid–base free energy of interaction between two surfaces at $h = h_o$ (i.e., at "contact"), λ_{AB} [nm] is the decay (Debye) length of water, which has been reported to range from 0.4 to 32 nm [55]. For this work, it was assumed that $\lambda_{AB} = 1$ nm [54], and $h_o = 0.25$ nm.

Currently, there are two approaches for the estimation of $\Phi_{AB(h=h_0)}$. The first approach is theoretical, developed by van Oss [74] and it is based on the surface tension electron-acceptor and electron-donor parameters of the individual materials; whereas, the second approach is empirical, developed by Yoon et al. [55] and it is based on the determination of the degree of hydrophobicity using water contact angles. In this study, the Yoon et al. [55] approach is employed:

$$\Phi_{AB(h=h_0)} = -\frac{K_{123}}{2\pi h_0\lambda_{AB}} \quad (18)$$

where K_{123} [J] is the hydrophobic force constant, which can be predicted by the following empirical relationship:

$$\log K_{123} = -7.0\left(\frac{\cos\beta_1+\cos\beta_3}{2}\right) - 18.0 \quad (19)$$

where β_1 [°] and β_3 [°] are the water contact angles of materials "1" and "3", respectively. Bergendahl and Grasso [76] compared the two methods for the estimation of $\Phi_{AB(h=h_0)}$ and found that they lead to quite similar results. In this study, the following contact angles were employed: $\beta_{MS2} = 33\pm1°$, $\beta_{\Phi X174} = 26\pm1.7°$ [40], $\beta_{KGa\text{-}1b} = 46.1°$, and $\beta_{STx\text{-}1} = 20.5\pm2.8°$ [78].

4. Results and discussion

4.1. Batch experiments

The experimental data from the equilibrium attachment experiments of MS2 and ΦX174 onto KGa-1b and STx-1b are shown in Fig. 7, and they were fitted with a Freundlich type isotherm:

$$C_{eq}^* = K_f C_{eq}^m \quad (20)$$

where C_{eq}^* [(M viruses)/(M clay)] is the virus concentration attached onto clay colloids at equilibrium in units of (PFU/μg clay), C_{eq} [M/L^3] is the aqueous phase virus concentration at equilibrium in units of (PFU/mL), K_f [(L^3/M)^m] is the Freundlich constant in units of {(mL)^m/[(μg clay)(PFU)$^{m-1}$]}, and m [–] is the Freundlich exponent. The parameters K_f and m were estimated by linear regression of the log-transformed data:

$$\log C_{eq}^* = \log K_f + m\log C_{eq} \quad (21)$$

The greater the value of K_f, the higher the affinity of viruses for clay minerals. The Freundlich isotherm parameters for the attachment experiments conducted in this study are listed in Table 2. Worthy to note is that for all cases considered in this study the value of the Freundlich exponent m is close to unity, suggesting

Table 2
Freundlich isotherm parameter values.

Interacting materials	K_f (mL/μg)^m	m
ΦX174 & KGa-1b	$2.26 \times 10^{-3} \pm 7.6 \times 10^{-4}$	1.00 ± 0.02
MS2 & KGa-1b	$4.34 \times 10^{-3} \pm 2.8 \times 10^{-3}$	0.93 ± 0.07
ΦX174 & STx-1b	$2.71 \times 10^{-4} \pm 8.2 \times 10^{-5}$	1.12 ± 0.02
MS2 & STx-1b	$7.58 \times 10^{-4} \pm 2.1 \times 10^{-4}$	1.06±0.02

that the a linear type isotherm employed in other studies [7] could also be an acceptable model. The experimental results suggested that the affinity of both bacteriophages (ΦX174 and MS2) is greater for KGa-1b than STx-1b. It should be noted that this observation is in agreement with the work by Schiffenbauer and Stotzky [4] who have reported that the attachment of coliphages T7 and T1 is greater onto kaolinite than montmorillonite. Furthermore, it was observed that the attachment of MS2 onto both minerals was greater than that of ΦX174. The reason that the attachment of ΦX174 onto STx-1b was smaller than the attachment onto KGa-1b is attributed to the more negatively charged surfaces of STx-1b, which yielded stronger repulsive forces. These results are consistent with the work by Syngouna and Chrysikopoulos [7], who observed that MS2 exhibits greater affinity for clay particles than ΦX174. However, Lipson and Stotzky [49] reported that more reovirus particles were attached onto montmorillonite than onto kaolinite, suggesting that the mechanisms of attachment differ for different viruses.

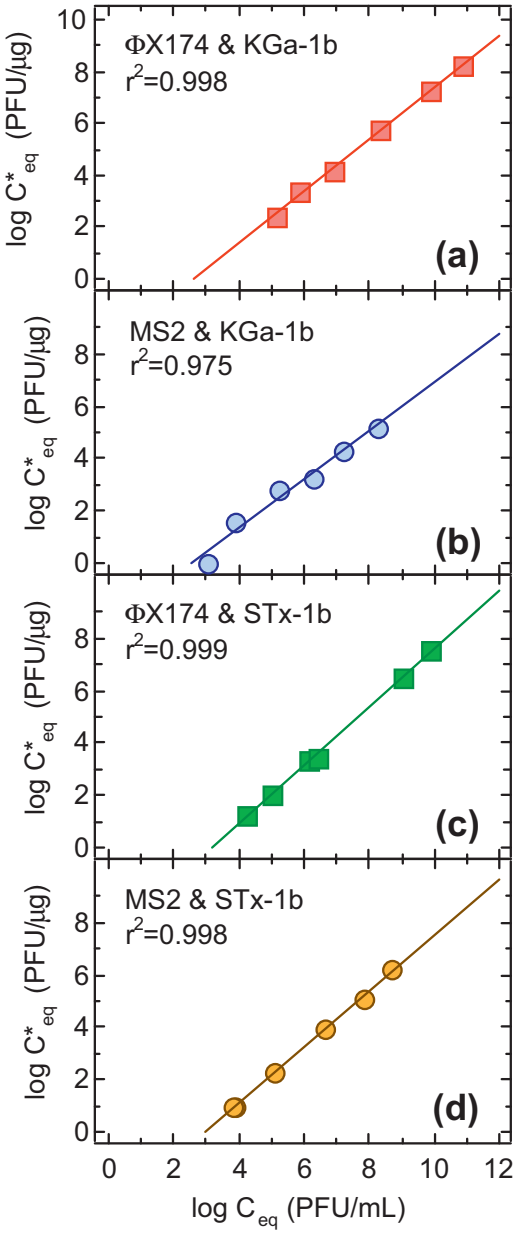

Fig. 7. Freundlich isotherms for the attachment of (a) ΦX174 onto KGa-1b, (b) MS2 onto KGa-1b, (c) ΦX174 onto STx-1b, and (d) MS2 onto STx-1b at pH 7.0 and 25 °C. The corresponding Freundlich parameters K_f and m are listed in Table 2.

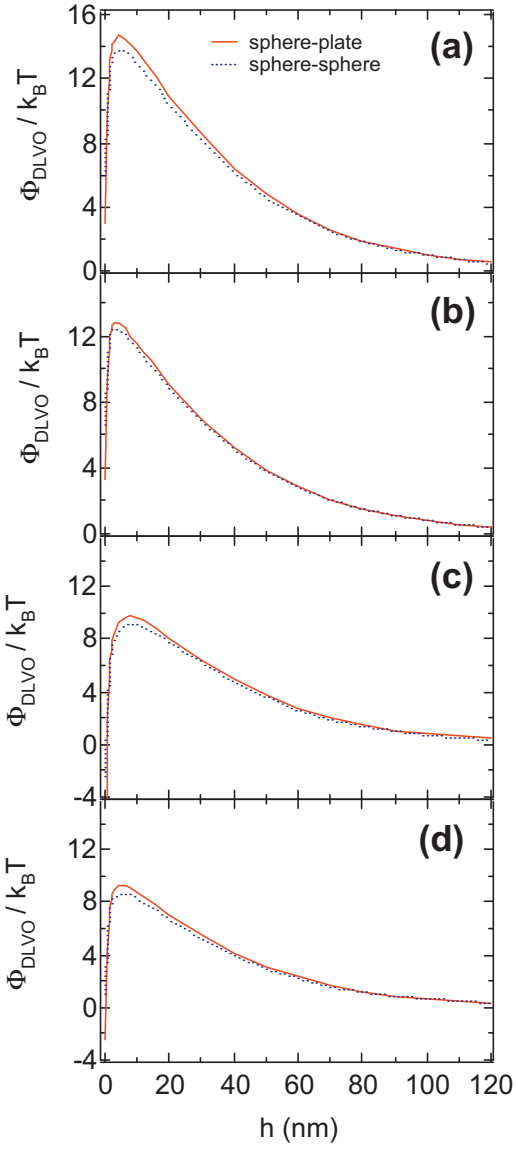

Fig. 8. Predicted DLVO interaction energy profiles for (a) MS2 with KGa-1b, (b) ΦX174 with KGa-1b, (c) MS2 with STx-1b, and (d) ΦX174 with STx-1b as a function of separation distance for the experimental conditions, using both sphere-plate and sphere-sphere approximations.

4.2. Calculations of virus–clay interactions

In this study, viruses were considered to follow the principles of colloid chemistry, despite the fact that they are more complex than abiotic colloids [79]. Theoretically, a DLVO interaction energy profile is characterized by a deep energy "well", which appears at relatively small separation distances and it is known as the primary minimum, Φ_{min1}, the energy barrier to attachment and detachment known as the primary maximum, Φ_{max1}, and a shallow energy "well" at relatively large separation distances known as

Table 3
Calculated Φ_{max1}, Φ_{min1}, and Φ_{min2} values for sphere–plate and sphere–sphere models using DLVO and XDLVO theories and the experimental conditions (pH = 7, $I_s = 10^{-4}$ M).

	KGa-1b						STx-1b					
	Sphere–plate			Sphere–sphere			Sphere–plate			Sphere–sphere		
	Φ_{max1} (k_BT)	Φ_{min1} (k_BT)	Φ_{min2} (k_BT)	Φ_{max1} (k_BT)	Φ_{min1} (k_BT)	Φ_{min2} (k_BT)	Φ_{max1} (k_BT)	Φ_{min1} (k_BT)	Φ_{min2} (k_BT)	Φ_{max1} (k_BT)	Φ_{min1} (k_BT)	Φ_{min2} (k_BT)
DLVO theory												
MS2	14.7	na[a]	-1.2×10^{-4}	13.8	na[a]	−0.013	9.8	−5.8	-1.3×10^{-3}	9.2	−2.5	−0.015
ΦX174	13.2	na[a]	-1.3×10^{-4}	12.4	na[a]	−0.014	9.3	−2.4	-1.4×10^{-3}	8.7	na[a]	−0.019
XDLVO theory												
MS2	12.0	-7.3×10^{5}	-1.2×10^{-4}	11.4	-7.14×10^{5}	−0.013	9.3	-2.1×10^{4}	-1.3×10^{-3}	8.7	-2.1×10^{4}	−0.015
ΦX174	11.6	-3.7×10^{3}	-1.3×10^{-4}	10.9	-3.62×10^{3}	−0.014	9.1	-1.1×10^{2}	-1.4×10^{-3}	8.5	-1.0×10^{2}	−0.019

[a] No primary minimum depth, Φ_{min1} can not be calculated.

Table 4
Calculated values of $\Phi_{AB(h=h_0)}$ based on the empirical approach reported by Yoon et al. [55].

Surface	$\Phi_{AB(h=h_0)}$ (mJ/m^2)
	MS2
KGa-1b	−39,044
STx-1b	−1122
	ΦX174
KGa-1b	−191
STx-1b	−5.48

Table 5
Parameter values employed in the theoretical considerations.

Parameter	Values	References
A_{123}	7.5×10^{-21} J	[72]
λ	10^{-7} m	[63]
r_p	MS2: 12.5×10^{-9} m	[57], this study
	ΦX174: 13×10^{-9} m	[57], this study
	KGa-1b: $4.21 \times 10^{-7} \pm 6.29 \times 10^{-8}$ m	this study
	STx-1b: $5.94 \times 10^{-7} \pm 1.90 \times 10^{-9}$ m	this study
$\varepsilon_r = \varepsilon/\varepsilon_0$	78.4 (–)	[80]
ε_0	8.854×10^{-12} C^2/(J·m)	[80]
ζ	MS2: −0.040 V	this study
	ΦX174:−0.032 V	this study
	KGa-1b: −0.026 V	this study
	STx-1b: −0.021 V	this study
κ^{-1}	3.06×10^{-8} m	this study
I_s	0.0001 mol/L	this study
N_A	6.0221367×10^{23} 1/mol	[80]
e	1.602×10^{-19} C	[80]
k_B	1.381×10^{-23} J/K	[80]
T	298	this study
σ_{Born}	5 Å	[67]
λ_{AB}	1 nm	[54]
β_{MS2}	$33 \pm 1^\circ$	[40]
$\beta_{\Phi X174}$	$26 \pm 1.7^\circ$	[40]
β_{KGa-1b}	46.1°	[78]
β_{STx-1b}	$20.5 \pm 2.8^\circ$	[78]

the secondary minimum, Φ_{min2} [43]. Interaction energy profiles for all possible virus-clay interactions were calculated using classical DLVO theory for both sphere-plate as well as sphere-sphere cases for the experimental conditions (pH = 7, $I_s = 10^{-4}$ M). The results are shown in Fig. 8. The Φ_{dl} values were calculated using Eq. (7) for sphere-plate interactions or Eq. (13) for sphere-sphere interactions, and the electrokinetic zeta potentials instead of the surface potentials. For all cases considered in Fig. 8, the DLVO interaction energies are highly repulsive for relatively long separation distances. The interaction energy profiles for the bacteriophages with KGa-1b do not exhibit a Φ_{min1}, but only a shallow Φ_{min2} (see Fig. 8a and b), indicating unfavorable attachment (bacteriophages attach onto KGa-1b surfaces in the secondary energy minimum). However, Φ_{min1} were observed in the interaction energy profiles for the bacteriophages with STx-1b, which suggests that bacteriophages could adhere onto clays if they have sufficient kinetic energy to overcome the potential energy barrier. All calculated Φ_{max1}, Φ_{min1}, and Φ_{min2} are listed in Table 3. Worthy to note is that Φ_{max1} values are slightly higher for MS2 than ΦX174 interactions with both minerals, and higher for sphere–plate than sphere–sphere models (see Table 3). Although, both sphere–plate and sphere–sphere particle

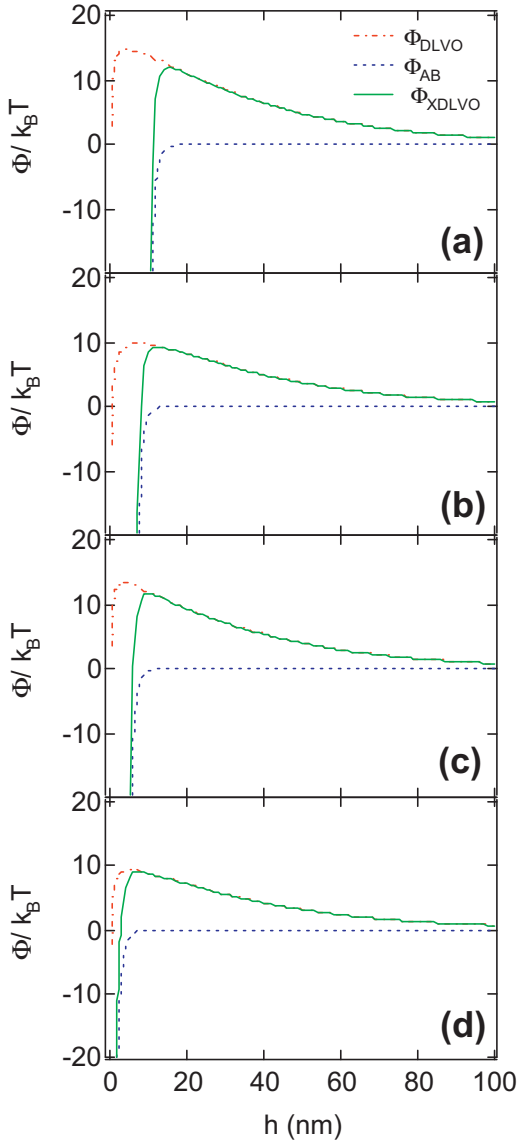

Fig. 9. Predicted sphere-plate Φ_{DLVO}, Φ_{AB}, and Φ_{XDLVO} interaction energy profiles for (a) MS2 and KGa-1b, (b) MS2 and STx-1b, (c) ΦX174 and KGa-1b, and (d) ΦX174 and STx-1b as a function of separation distance, for the experimental conditions.

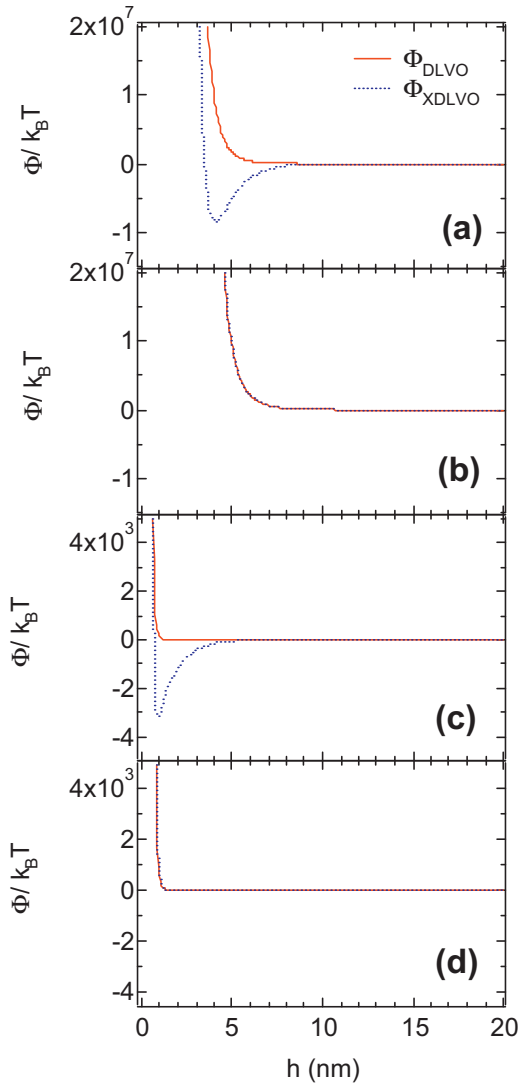

Fig. 10. Predicted sphere-sphere Φ_{DLVO}, and Φ_{XDLVO} interaction energy profiles for (a) KGa-1b-KGa-1b, (b) STx-1b-STx-1b, (c) MS2-MS2, and (d) ΦX174-ΦX174 as a function of separation distance, for the experimental conditions.

geometry models lead to comparable results, given that the size of bacteriophages is orders of magnitude smaller than the size of minerals used in this study, the sphere–plate model is considered a more appropriate model.

4.3. XDLVO calculations

In order to evaluate the relative contribution of the Lewis acid–base interaction energy to the XDLVO, the Φ_{DLVO}, Φ_{AB}, and Φ_{XDLVO} profiles were calculated for the case of sphere–plate approximation and all possible virus–clay interactions under the experimental conditions of this study (pH = 7, $I_s = 10^{-4}$ M). For the evaluation of $\Phi_{AB(h=h_0)}$ the empirical approach (18) proposed by Yoon et al. [55] was employed with hydrophobic force constants predicted by the empirical relationship (19). The various $\Phi_{AB(h=h_0)}$ values calculated are listed in Table 4. Furthermore, the various parameters used in the theoretical considerations are listed in Table 5. Furthermore, the predicted interaction energy profiles are shown in Fig. 9. Also, the various Φ_{max1}, Φ_{min1}, and Φ_{min2} calculated values are listed in Table 3. Clearly, in most cases, the Φ_{XDLVO} profiles exhibit a deep primary energy minimum, suggesting that Lewis acid–base interactions play an important role in the total interaction energy, and that they work to the advantage of MS2 and ΦX174 attachment onto the selected clay minerals. Comparison of the depths of primary minimum for each virus–water-collector system, the magnitudes of primary energy minimum were found to be greater for MS2 than ΦX174. Furthermore, the Φ_{min1} for both viruses was greater for KGa-1b than STx-1b. Overall, maximum Φ_{min1} was observed for MS2 interaction with KGa-1b, which is in agreement with the experimental results of this study (see Fig. 7 and Table 2). Furthermore, comparison of the Φ_{DLVO} and Φ_{XDLVO} interaction energy profiles shown in Fig. 9 indicates that taking into account the Lewis acid–base interactions the energy barriers are reduced at longer separation distances. Note that the calculated Φ_{max1} values are smaller for Φ_{XDLVO} than Φ_{DLVO} for all cases considered (see Table 3).

Clearly, Φ_{AB} hydrophobic interaction energy profiles significantly influence the DLVO profiles. Worthy to note is that $\Phi_{AB(h=h_0)}$ values are more negative for MS2 than ΦX174 interactions with the clays and more negative for KGa-1b than STx-1b interactions with both viruses (see Table 4). These findings are in agreement with the experimental results of this study (see Fig. 7 and Table 2), showing that the degree of virus attachment onto KGa-1b was greater than that onto STx-1b. Therefore, the XDLVO theory can successfully explain the hydrophobic interaction-mediated attachment of MS2 and ΦX174 onto KGa-1b and STx-1b.

4.4. Particle aggregations

In order to evaluate the possibility of particle aggregation, the Φ_{DLVO} and Φ_{XDLVO} interaction energy profiles for the case of sphere-sphere approximation as applied to identical virus–virus and clay–clay interactions were constructed under the experimental conditions ($I_s = 0.0001$ M, pH = 7) and are shown in Fig. 10. Clearly, the classical DLVO theory suggests that, for all cases considered, no coagulation between like particles is expected to occur under the experimental conditions. However, the XDLVO theory predicts a primary minimum for KGa-1b–KGa-1b and MS2–MS2 cases, and suggests that hydrophobic interactions between MS2 particles or KGa-1b particles could lead to initial aggregation.

5. Conclusions

Our results showed that MS2 and ΦX174 attachment onto KGa-1b and STx-1b is adequately described by the Freundlich isotherm equation. Both MS2 and ΦX174 were attached in greater amounts onto KGa-1b than STx-1b. Lewis acid–base interactions play an important role in the total interaction energy, and certainly, can successfully explain the hydrophobic interaction-mediated attachment of MS2 and ΦX174 onto KGa-1b and STx-1b. Furthermore, hydrophobic interactions between MS2 particles or KGa-1b particles could lead to initial aggregation at pH = 7 and $I_s = 10^{-4}$ M.

Acknowledgments

This research has been co-financed by the European Union (European Social Fund-ESF) and Greek national funds through the Operational program “Education and Lifelong Learning” of the National Strategic Reference Framework (NSRF)-Research Funding Program: Heracleitus II. Investing in knowledge society through the European Social Fund.

References

[1] M.V. Yates, C.P. Gerba, L.M. Kelly, Appl. Environ. Microbiol. 49 (1985) 778.
[2] R. Anders, C.V. Chrysikopoulos, Water Resour. Res. 41 (2005), W10415, doi: 10.1029/2004WR003419.
[3] R.J. Hunt, M.A. Borchard, K.D. Richards, S.K. Spencer, Environ. Sci. Technol. 44 (2010) 7956.

[4] M. Schiffenbauer, G. Stotzky, Appl. Environ. Microbiol. 43 (1982) 590.
[5] D. Jiang, Q. Huang, P. Cai, X. Rong, W. Chen, Colloids Surf. B: Biointerfaces 54 (2007) 217.
[6] X. Rong, Q. Huanga, X. He, H. Chen, P. Cai, W. Liang, Colloids Surf. B: Biointerfaces 64 (2008) 49.
[7] V.I. Syngouna, C.V. Chrysikopoulos, Environ. Sci. Technol. 44 (2010) 4539.
[8] I.A. Vasiliadou, D. Papoulis, C.V. Chrysikopoulos, D. Panagiotaras, E. Karakosta, M. Fardis, G. Papavassiliou, Colloids Surf. B: Biointerfaces 84 (2011) 354.
[9] G.E. Walshe, L. Pang, M. Flury, M.E. Close, M. Flintoft, Water Res. 44 (2010) 1255.
[10] I.A. Vasiliadou, C.V. Chrysikopoulos, Water Resour. Res. 47 (2011), W02543, doi:1029/2010WR009560.
[11] A. Abdel-Salam, C.V. Chrysikopoulos, J. Hydrol 165 (1995) 261.
[12] A. Abdel-Salam, C.V. Chrysikopoulos, Transport Porous Media 20 (1995) 197.
[13] M.E. Tatalovich, K.Y. Lee, C.V. Chrysikopoulos, Transport Porous Media 38 (2000) 93.
[14] J.E. Saiers, Water Resour. Res. 38 (2002), 110.1029/2001WR000320.
[15] M.Y. Corapcioglu, S.Y. Jiang, Water Resour. Res. 29 (1993) 2215.
[16] D. Grolimund, M. Borkovec, Environ. Sci. Technol. 39 (2005) 6378.
[17] H.M. Bekhit, A.E. Hassan, Adv. Water Resour. 28 (2005) 1320.
[18] H.M. Bekhit, A.E. Hassan, Water Resour. Res. 43 (2007), W08409, doi:1029/206WR005418.
[19] S.C. James, T.K. Bilezikjian, C.V. Chrysikopoulos, Stoch. Environ. Res. Risk Assess. 19 (2005) 266.
[20] J. Simunek, C.M. He, L.P. Pang, S.A. Bradford, Vadose Zone J. 5 (2006) 1035.
[21] A. Massoudieh, T.R. Ginn, J. Contam. Hydrol. 92 (2007) 162.
[22] M. Flury, H. Qiu, Vadose Zone J. 7 (2008) 682.
[23] N. Natarajan, G.S. Kumar, Colloids Surf. A: Physicochem. Eng. Aspects 370 (2010) 49.
[24] V.V. Nair, S.G. Thampi, Colloids Surf. A: Physicochem. Eng. Aspects 373 (2011) 74.
[25] Y. Jin, M.V. Yates, S.S. Thompson, W.A. Jury, Environ. Sci. Technol. 31 (1997) 548.
[26] Y. Sim, C.V. Chrysikopoulos, Water Resour. Res. 32 (1996) 2607.
[27] Y. Sim, C.V. Chrysikopoulos, Adv. Water Resour 22 (1999) 507.
[28] R.W. Harvey, J.N. Ryan, FEMS Microbiol. Ecol. 49 (2004) 3.
[29] T.K. Sen, Water Air Soil Pollut. 216 (2011) 239.
[30] Y. Sim, C.V. Chrysikopoulos, Water Resour. Res. 31 (1996) 1429, Correction, Water Resour. Res. 32 (1996) 1473.
[31] C.V. Chrysikopoulos, Y. Sim, J. Hydrol. 185 (1996) 199.
[32] Y. Sim, C.V. Chrysikopoulos, Transport Porous Media 30 (1998) 87.
[33] Y. Sim, C.V. Chrysikopoulos, Water Resour. Res. 36 (2000) 173.
[34] J.F. Schijven, J. Simunek, J. Contam. Hydrol. 55 (2002) 113.
[35] C.V. Chrysikopoulos, E.T. Vogler, Stoch. Environ. Res. Risk Assess. 18 (2004) 67.
[36] S. Sirivithayapakorn, A.A. Keller, Water Resour. Res. 39 (1109) (2003), doi:10.1029/2002WR001583.
[37] A.A. Keller, S. Sirivithayapakorn, C.V. Chrysikopoulos, Water Resour. Res. 40 (2004), W08304, doi:10.1029/2003WR002676.
[38] S. Torkzaban, S.M. Hassanizadeh, J.F. Schijven, H.A.M. de Bruin, A.M. de Roda Husman, Vadose Zone J. 5 (2006) 877.
[39] R. Anders, C.V. Chrysikopoulos, Transport Porous Media 76 (2009) 121.
[40] R. Attinti, J. Wei, K. Kniel, J.T. Sims, Y. Jin, Environ. Sci. Technol. 44 (2010) 2426.
[41] C.V. Chrysikopoulos, C. Masciopinto, R. La Mantia, I.D. Manariotis, Environ. Sci. Technol. 44 (2010) 971.
[42] G. Sadeghi, J.F. Schijven, T. Behrends, S.M. Hassanizadeh, J. Gerritse, P.J. Kleingeld, Ground Water 49 (2011) 12.
[43] V.I. Syngouna, C.V. Chrysikopoulos, J. Contam. Hydrol. 126 (2011) 301.
[44] J.F. Schijven, W. Hoogenboezem, S.M. Hassanizadeh, J.H. Peters, Water Resour. Res. 35 (1999) 1101.
[45] J.F. Schijven, G. Medema, A.J. Vogelaar, S.M. Hassanizadeh, J. Contam. Hydrol. 44 (2000) 301.
[46] W.W. Woessner, P.N. Ball, D.C. DeBorde, T.L. Troy, Ground Water 39 (2001) 886.
[47] R.M. Maxwell, C. Welty, A.F.B. Tompson, Adv. Water Res. 26 (2003) 1075.
[48] C. Masciopinto, R. La Mantia, C.V. Chrysikopoulos, Water Resour. Res. 44 (2008) WR005643, W01404, doi: 10. 1029/2006.
[49] S.M. Lipson, G. Stotzky, Appl. Environ. Microbiol. 46 (1983) 673.
[50] J.P. Loveland, S. Bhattacharjee, J.N. Ryan, M. Elimelech, J. Contam. Hydrol. 65 (2003) 161.
[51] S. Chattopadhyay, R.W. Puls, Environ. Sci. Technol. 33 (1999) 3609.
[52] B.V. Derjaguin, L. Landau, Acta Physicochim. USSR 14 (1941) 633.
[53] E.J. Verwey, J.T.G. Overbeek, Theory of the stability of lyophobic colloids, Elsevier, Amsterdam, 1948.
[54] C.J. van Oss, Colloids Surf. A: Physicochem. Eng. Aspects 78 (1993) 1.
[55] R.-H. Yoon, D.H. Flin, Y.I. Rabinovich, J. Colloid Interface Sci. 185 (1997) 363.
[56] L.S. Dorobantu, S. Bhattacharjee, J.M. Foght, M.R. Gray, Langmuir 25 (2009) 6968.
[57] P.A. Shields, Factors influencing virus adsorption to solids, Ph.D. Dissertation, University of Florida, Gainesville, FL, 1986.
[58] M.H. Adams, Bacteriophages, Interscience, New York, 1959.
[59] R.J. Pruett, H.L. Webb, Clays Clay Miner. 41 (1993) 514.
[60] H. van Olphen, J.J. Fripiat, Data Handbook for Clay Minerals and Other Nonmetallic Minerals, Pergamon Press, Oxford, England, 1979.
[61] R.L. Sanders, N.M. Washton, K.T. Mueller, J. Phys. Chem. C 114 (2010) 5491.
[62] J.P. Loveland, J.N. Ryan, G.L. Amy, R.W. Harvey, Colloids Surf. A: Physicochem. Eng. Aspects 107 (1996) 205.
[63] J. Gregory, J. Colloid Interface Sci. 83 (1981) 138.
[64] J.N. Israelachvili, Intermolecular and Surface Forces, 2nd ed., Academic Press, London, 1992.
[65] W. Norde, Colloids and Intrfaces in Life Sciences, Marcel Dekker, New York, 2003.
[66] R. Hogg, T.W. Healy, D.W. Fuerstenau, Trans. Faraday Soc 62 (1966) 1638.
[67] E. Ruckenstein, D.C. Prieve, AIChE J. 22 (1976) 276.
[68] G. Frens, J.T.G. Overbeek, J. Colloid Interface Sci. 38 (1972) 376.
[69] N. Kallay, B. Biskup, M. Tomic, E. Matijevic, J. Colloid Interface Sci. 114 (1986) 357.
[70] D.L. Feke, N.D. Prabhu, J.A. Mann Jr., J.A. Mann III, J. Phys. Chem. 88 (1984) 5735.
[71] J.N. Ryan, P.M. Gschwend, J. Colloid Interface Sci. 164 (1994) 21.
[72] J.P. Murray, G.A. Parks, in: M.C. Kavanaugh, J.O. Leckie (Eds.), Particulates in Water: Characterization, Fate, Effects and Removal, Advances in Chemistry Series 189, American Chemical Society, Washington, DC, 1978.
[73] B.E. Novich, T.A. Ring, Clays Clay Miner. 32 (1984) 400.
[74] C.J. van Oss, Interfacial Forces in Aqueous Media, Marcel Dekker, New York, 1994.
[75] S.W. Swanton, Adv. Colloid Interface Sci. 54 (1995) 129.
[76] J. Bergendahl, D. Grasso, AIChE J. 45 (1999) 475.
[77] C.J. van Oss, R.F. Giese, J. Dispers. Sci. Technol. 25 (2004) 631.
[78] W. Wu, Clays Clay Miner. 49 (2001) 446.
[79] M.C.M. van Loosdrecht, J. Lyklema, W. Norde, A.J.B. Zehnder, Microb. Ecol. 17 (1989) 1.
[80] CRC, in: R.C. Weast (Ed.), Handbook of Chemistry and Physics, 64th ed., CRC Press, 1984.